Pluto's Atmosphere from the May 22, 2011 Stellar Occultation

by

Stephanie E. Sallum

Submitted to the Department of Earth, Atmospheric and Planetary Sciences

in Partial Fulfillment of the Requirements for the Degree of

Bachelor of Science in Earth, Atmospheric and Planetary Sciences

at the Massachusetts Institute of Technology

May 11, 2012 [June 2012]

Author Signature redacted

Stephanie E. Sallum
Department of Earth, Atmospheric and Planetary Sciences
May 11, 2012

Certified by Signature redacted

Richard P. Binzel
Thesis Supervisor

Accepted by Signature redacted

Samuel Bowring
Chair, Committee on Undergraduate Program

Abstract

This paper reports the observations and atmospheric fitting results from the May 22, 2011 stellar occultation by Pluto. Of the nine sites across the United States that attempted to observe the event, three obtained light curves at the predicted midtime without being clouded out. Simultaneous fitting of these three light curves utilizing a model fully detailed in Elliot and Young [1992] resulted in a best fit half-light radius of 1309 $\pm$ 25 km, a calculated temperature of 94 $\pm$ 4 K, and a calculated pressure scale height of 55 $\pm$ 2 km. These parameters, in the context of the previous occultations, reveal a trend in which Pluto's half-light radius has been increasing slightly since an initial dramatic increase between 1988 and 2002. While the pressure scale height has remained relatively constant, the temperature has decreased slightly over the recorded events. The changes in half-light radius agree with frost migration models in which Pluto's surface has a low thermal inertia [Hansen and Paige, 1996; Elliot et al., 2007], but further constraints on frost migration model parameters such as substrate and frost albedo, frost emissivity, and the supply of N_2 require additional observations. The *New Horizons* spacecraft should encounter a dynamic atmosphere on Pluto during the scheduled fly by in 2015.

Acknowledgements

I would like to thank several members of MIT's Planetary Astronomy Lab (PAL): Dr. Michael Person, for advising me throughout this project, Dr. Amanda Bosh, for all her help with occultation observations, Carlos Zuluaga, for supervising me during my first year at PAL, Tim Brothers, for his help when I was learning to observe (especially during 12.410), and Amanda Zangari, for all the answered questions and IRAF tutorials. I would like to give a special thanks to the late Professor Jim Elliot, for introducing me to astronomy and giving me my first UROP at PAL and Professor Richard Binzel, for all his help with applications and advising me during the last year. I would also like to thank Brian Taylor and Jessie Runnoe, for observing at WIRO with me, and Chip Kobulnicky and James Weger for hosting us at WIRO.

Contents

List of Figures

List of Tables

Chapter 1

Introduction

To date, stellar occultations have provided astronomers with the most detailed record of the size and behavior of Pluto's atmosphere over time. Observations of a stellar occultation by Pluto occurring June 9, 1988 [Elliot et al., 1989] yielded the first detection of an atmosphere thought to be composed of N_2, CH_4, or CO. In the following 24 years, five subsequent occultations have allowed for more extensive study of Pluto's atmospheric behavior [Elliot et al., 1989; Sicardy et al., 2003; Pasachoff et al., 2005; Elliot et al., 2007; Person et al., 2008]. Table 1.1 lists the results of these five events.

The June 9, 1988 occultation resulted in the first determination of Pluto's pressure scale height, at 56 ± 5 km [Millis et al., 1993][1] and also sparked an interest in Pluto's atmospheric composition. Yelle and Lunine [1989] examined the energy balance in the atmosphere, and found that the mean molecular weight was approximately 25 amu with an atmospheric temperature of 100 K at 1 μbar, leading them to believe Pluto's atmosphere to be composed of methane and some heavier molecule: either argon, molecular nitrogen, or carbon monoxide. Spectroscopic study by Owen et al. [1993], calculating abundances from absorption features due to carbon monoxide, methane, and molecular nitrogen ices, determined Pluto's main atmospheric constituent to be molecular nitrogen.

[1]Millis et al. [1993] led to the reexamination and publication of a 1985 occultation by Brosch [1995], which indicated Pluto possessed an atmosphere prior to the 1988 event.

The shape of the 1988 light curve raised questions regarding Pluto's atmospheric structure. A "kink" (see Figure 1.1) in the occultation light curve consisting of an upper slope consistent with an isothermal, clear atmosphere, followed by a more abrupt drop in flux revealed the presence of two layers in Pluto's atmosphere [Elliot et al., 1989]. Elliot et al. [1989] hypothesized the second, sharper slope to result from either an extinction layer or refraction associated with a sharp thermal gradient, and used an empirical model to fit the 1988 light curve for Pluto's upper atmospheric structure.

The question of whether Pluto's lower atmosphere is dominated by extinction or thermal inversion has been left unanswered. Following the initial 1988 event, investigation of the nature of the lower layer proceeded with Hubbard et al. [1990] and Stansberry et al. [1994], who produced model light curves and showed that a strong thermal inversion layer could result in the minimum flux measured by the Kuiper Airborne Observatory (KAO) during the 1988 occultation. Utilizing radio occultation data taken with Viking, Eshleman [1989] argued that the shape of the 1988 occultation light curve was consistent with a radial change in refractive gradient, perhaps associated with a sharp thermal gradient. These three studies supported the hypothesis that Pluto's lower layer is indeed dominated by a sharp thermal gradient.

An occultation occurring on August 21, 2002 provided an opportunity to investigate this question further. Elliot et al. [2003b] recorded this event over the 0.75-2.2 μm wavelength range, plotting the residual stellar flux at the occultation midtime as a function of wavelength. The data revealed a greater residual flux at higher wavelengths, a trend consistent with atmospheric extinction by sub-micrometer-sized particles, which could not have been produced by a thermal inversion layer. Additionally, the shapes of the June 9, 1988 and August 21, 2002 occultation light curve (with the 1988 data manifesting a more abrupt change in slope - see Figure 1.2 for direct comparison of the three event profiles) implied a decrease in atmospheric extinction between the two events [Elliot et al., 2007]. Observations of another stellar occultation by Pluto on June 12, 2006 supported this, and Elliot et al. [2007] suggested that an event causing increased extinction in Pluto's atmosphere occurred prior to 1988 and that since then the atmosphere had been clearing. While these three events

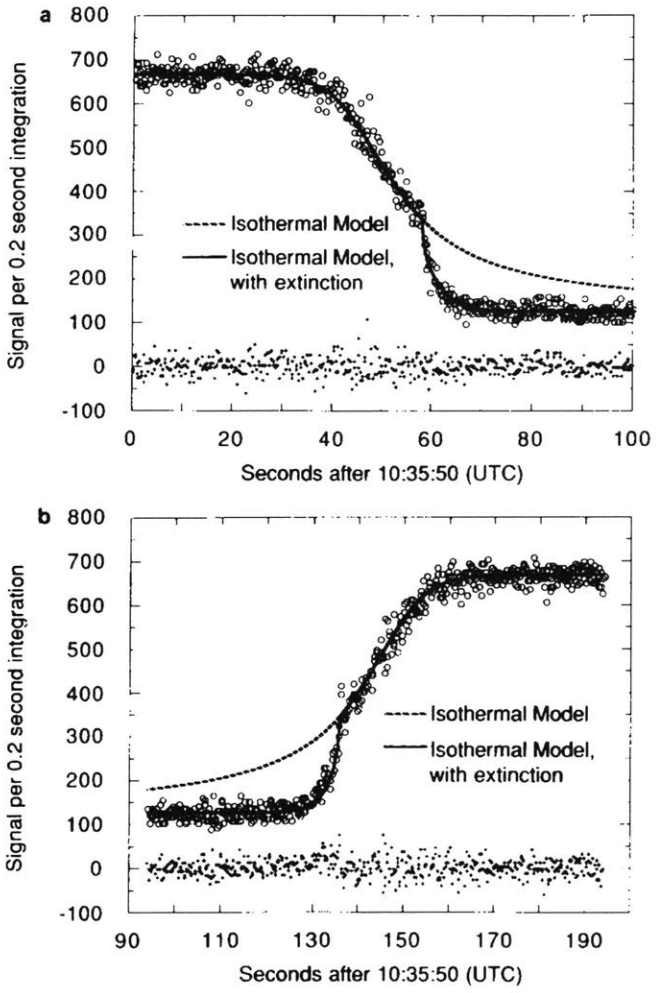

Figure 1.1: ***1988 Occultation Immersion and Emersion*** *Figure 3 from Elliot et al. [1989].* ***Top Panel (a):*** *immersion.* ***Bottom Panel (b):*** *emersion. Open circles represent data, and the dashed line models an isothermal atmosphere with a scale height of 59.7km. The solid line represents an atmospheric model in which extinction begins abruptly at a radius of 1189 ± 20km. The crosses plotted at the bottom of the figure represent residuals (data - model) Note the abrupt change in slope at half-light.*

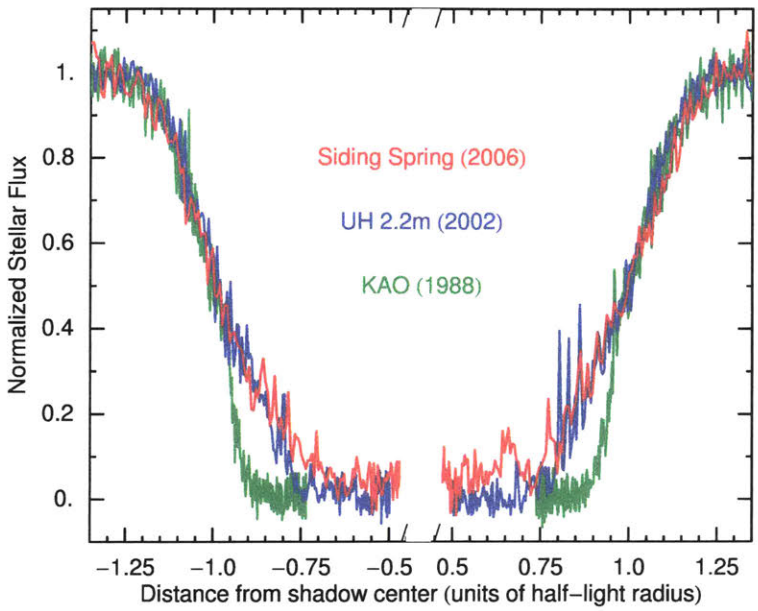

Figure 1.2: ***1988 - 2006 Changes in Slope*** *Figure 6 from Elliot et al. [2007]. Highest SNR light curves from the 1988, 2002, and 2006 occultations plotted simultaneously. Note the evolution of the light curves from an abrupt drop in 1988 to a more rounded one in 2006.*

revealed large changes in shadow size (and thus atmospheric structure below radii of ∼1230km) between 1988 and 2002, the insignificant change in shadow size between 2002 and 2006 (from 1279 ± 5 km to 1276 ± 4 km) suggests only subtle atmospheric changes occurring in those 4 years.

Fitting the 2002 occultation for Pluto's upper (clear, isothermal) atmospheric layer revealed a doubling in pressure in the 1200-1280 km radius range since the 1988 occultation [Elliot et al., 2003b]. Sicardy et al. [2003] also measured this doubling in pressure. This change agreed with frost migration models of Pluto's atmosphere described in detail in Hansen and Paige [1996]. Hansen and Paige [1996] applied a thermal model (originally designed in 1992 for Titan) to Pluto to test whether observations could be explained by an N_2 atmosphere in equilibrium with surface frost. The authors assumed that frost would be condensed or sublimed at a rate that main-

tained global vapor pressure equilibrium, as well as mass and energy conservation. In most model runs, the authors found that Pluto's atmospheric pressure would continue to increase until 2000, and then begin to decrease around 2020. The pressure variations found by the authors occurred twice per Pluto year, the greater of the two as a result of the north polar cap sublimation just following perihelion, and the lesser associated with sublimation of the south polar cap just preceding perihelion. The fact that Pluto reached perihelion on September 15, 1989 [Millis et al., 1993], indicates that the observed pressure changes are in agreement with the model presented in Hansen and Paige [1996]. The models that best fit the observations were those in which Pluto's surface possessed low thermal inertia.

Observations of the March 18, 2007 Pluto occultation, described fully in Person et al. [2008] showed a slight increase in half light radius, with a value of 1291 $\pm$ 5 km. This result showed a significant (albeit less than the 1988 - 2002 change) increase in half light radius since June 12, 2006, perhaps indicating a third epoch in Pluto's atmospheric behavior. Additionally, the March 18, 2007 occultation provided a novel opportunity to probe Pluto's atmosphere over horizontal distances, since Pluto's upper atmosphere followed a grazing path as seen from the observing stations [Person et al., 2008]. The Multiple Mirror Telescope Observatory (MMTO) light curve displayed oscillations that were remarkably symmetric over the event midtime (and thus Pluto's center), especially at immersion and emersion. The authors interpreted these structures as gravity waves in Pluto's upper atmosphere that are coherent across at least 1200 km, a significant fraction of Pluto's half light radius [Person et al., 2008].

The initially large, and then more subtle increases in stellar occultation half light radii over the years indicate that the planned *New Horizons* spacecraft flyby in 2015 will reveal a dynamic atmosphere. Continued monitoring of Pluto's atmosphere via occultation observations will allow for better investigation of the mechanisms causing the changes in extinction and radius. This paper reports on atmospheric fitting from the May 22, 2011 occultation by the Pluto-Charon system. Since then, a Pluto-Charon occultation occurring on June 23, 2011 led to additional constraints on Pluto's atmosphere [Person et al., 2012 in prep.].

Table 1.1. Pluto's Upper Atmosphere: 1988 - 2007

Parameter	1988 June 9[a]	2002 August 2[a]	2006 June 12[b]	2007 March 18[c]
Half-light radius (km)[d,e]	1233 ± 4	1279 ± 5	1276 ± 4	1291 ± 5
Pressure scale height (km)[e,f]	56 ± 5	61 ± 4	54 ± 3	54.2 ± 0.2
Temperature (K)[e,f]	114 ± 10	108 ± 9	97 ± 5	95 ± 1

[a]After Person et al. [2008]

[b]From Elliot et al. [2007]

[c]From Person et al. [2008]

[d]In Pluto's atmosphere (not the shadow)

[e]At the half-light radius

[f]For an N_2 atmosphere

Chapter 2

Observations

2.1 Predictions and Sites Overview

The MIT Planetary Astronomy Laboratory and its collaborators at nine sites across the United States attempted observations of the 2011 May 22 occultation of the 15.3 magnitude star UCAC2 24680978 (2MASS 48057952; shown in Figure 2.1).

Figure 2.2 displays the predicted paths of Pluto and Charon based on measured star positions and offsets and MIT's Ephemeris Correction Model for Pluto. Due to the lack of potential stations with which to observe Charon, we focused observations on stations around Pluto's predicted path. Observers obtained data at Williams College (0.61 m), Middlebury College (0.61 m), Yerkes Observatory (1.04 m), Star View Hill Observatory (SVH; 0.64 m), Observatoire du Mont Megantic (OMM; 1.6 m), MONET North at McDonald Observatory (MONET; 1.2 m), and the Wyoming Infrared Observatory (WIRO; 2.3 m). Observers at the MIT George R. Wallace, Jr. Astrophysical Observatory (WAO; 0.61 m) and the Clay Center Observatory (CCO; 0.64 m) attempted to record the event, but inclement weather prevented data acquisition. Table 2.1 summarizes the observation sites ordered east to west by longitude.

Observations at WAO, CCO, Williams and WIRO utilized the Portable Occultation, Eclipse, and Transit System (POETS; Souza et al. [2006]; Gulbis et al [2008]), which allows for high speed image cadence and GPS triggering. All POETS observations were unfiltered; the estimated effective wavelength for POETS maximum

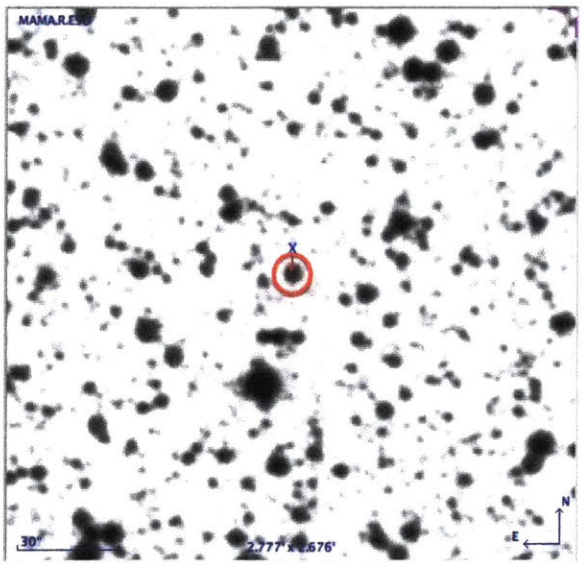

Figure 2.1: ***UCAC2 24680978 Finder*** *Finder chart for occultation star generated by Aladin Sky Atlas. The red circle indicates the target star.*

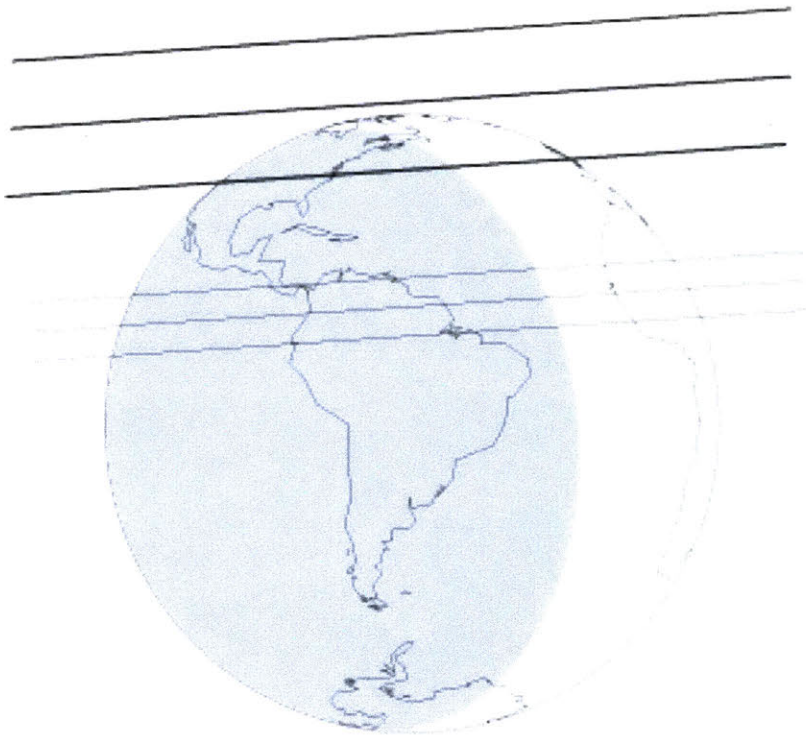

Figure 2.2: ***PC 20110522 Prediction Globe*** *Predicted paths of Pluto (upper bold track) and Charon (lower track). Generated by C. Zuluaga of the MIT Planetary Astronomy Laboratory.*

Figure 2.3: ***Map of Observation Sites*** *The map above marks the 9 sites at which observations were attempted as well as the one site that obtained normalization data. The black line marks the lower limit of Pluto's predicted path. The upper limit was off the globe and so is not shown in the figure. Generated by Google Maps.*

Table 2.1. Observational Sites

Site[a]	Telescope (m)	East Longitude (ddd mm ss)	Latitude (dd mm ss)	Altitude (km)	Observers
CCO	0.64	-71 08 14	42 18 27	0.1	Person
WAO	0.61	-71 29 06	42 36 36	0.11	Zangari
Middlebury	**0.61**	**-73 10 01**	**44 00 45**	**0.0**	**Briggs, Ratcliff, Winkler**
Williams	**0.61**	**-73 12 06**	**42 42 42**	**0.22**	**Pasachoff, Souza**
SVH	0.64	-74 56 45	40 57 41	0.22	Midkiff
OMM	1.6	-79 09 00	45 28 01	1.0	Bastien, Racine
Yerkes	**1.04**	**-88 33 22**	**42 34 13**	**0.0**	**Haislip, Hoette**
MONET	1.2	-104 01 21	30 40 17	2.08	Gulbis
WIRO	2.3	-105 58 34	41 05 49	2.94	Sallum, Taylor

[a]Successful observation sites shown in bold

sensitivity was 7400 ± 500 Å. WAO, Williams and WIRO data were taken in conventional (non-electron-multiplying) 1 MHz readout mode [Souza et al., 2006; Gulbis et al, 2008].

Middlebury and SVH observed using the Portable Instrument for Capturing Occultations (PICO) systems [Lockhart et al, 2006], which have a short readout time between frames and GPS triggering. Middlebury utilized 1.5 second exposures at a cadence of 4 seconds, and SVH 1 second exposures at a 2 second cadence. PICO observations were also unfiltered, with an estimated effective wavelength of 7400 ± 500 Å.

Observers at Yerkes recorded data using an unfiltered SBIG ST-L-1001 with 5 second exposures; the long readout time between frames resulted in a 12 second cadence. These data were unfiltered, with an estimated effective wavelength of 7400 ± 500 Å.

OMM recorded 8 second exposures at a 12.75 second cadence using *Camera Panoramique Roche InfraRoughe* (CPAPIR; Artigau et al. [2004]). These data were

Table 2.2. Instrumental Parameters

Site[a]	Instrument	Effective Wavelength (Å)	Cadence (Hz)
CCO	POETS	7400 ± 500 (unfiltered)	0.5
WAO	POETS	7400 ± 500 (unfiltered)	N/A
Middlebury	**PICO**	**7400 ± 500 (unfiltered)**	**0.25**
Williams	**POETS**	**7400 ± 500 (unfiltered)**	**0.5**
SVH	PICO	7400 ± 500 (unfiltered)	0.5
OMM	CPAPIR	8500 ± 100 (I filter)	0.08
Yerkes	**SBIG ST-L-1001**	**7400 ± 500 (unfiltered)**	**0.08**
MONET	ALTA E47+	6400 (unfiltered)	0.5
WIRO	POETS	7400 ± 500 (unfiltered)	0.2

[a]Successful observation sites shown in bold

recorded through an I filter, with an effective wavelength of 8500 ± 100 Å.

MONET used the ALTA E47+ camera to record 5 second exposures. I estimated the effective unfiltered wavelength for the ALTA E47+ camera to be 6400 ± Å from the CCD sensitivity plotted as a function of wavelength in the camera specifications. Table 2.2 displays the instrumental parameters for all observation sites (again ordered east to west by longitude).

2.2 WIRO

I observed with Brian Taylor, of Boston University, at WIRO, and thus am including a more detailed description of those observations. Jessie Runnoe, a University of Wyoming graduate student, assisted us in the telescope operations. As stated previously, we utilized a POETS system, and all data were recorded in the conventional 1 MHz, 16-bit mode. The University of Wyoming allocated us two nights at the observatory, and we used the first night to take test data in preparation for the actual event.

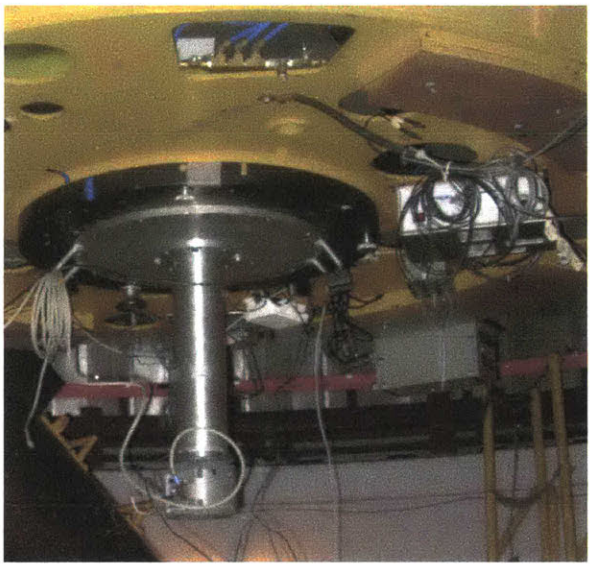

Figure 2.4: ***POETS Mounting*** *POETS mounted at WIRO. This image was actually taken during a subsequent KBO occultation, but the same setup was used to mount POETS for the May 22, 2011 Pluto event.*

After mounting the POETS system onto the telescope utilizing a custom boot fabricated at the University of Wyoming, shown in Figure 2.4, we began test observations at 7:36pm MST. We took a series of 100 flat frames followed by 100 bias frames, triggered internally (rather than by the GPS system), at 1x1 binning. The first two rows of Table 2.4 summarize these observations.

Due to WIRO's pointing inaccuracy, which manifested itself mostly as declination offsets and changed as a function of zenith angle, we decided on a set of bright stars to use to locate the occultation star. These stars were all brighter than magnitude 6, and ranged in approximate declination between 37° and -16°. Table 2.3 lists these stars and their coordinates. We practiced this star hopping on the night of the 21st, correcting the right ascension and declination offsets at each pointing. Pointing to HD 109085, with a declination of -16:11:00, (approximately 2° from the occultation star), resulted in an offset of 15s in right ascension, and 4m25s in declination. Using these offsets, we were able to point to zenith and back to HD 109085. After going through this process, we would have waited for the occultation star to rise and taken test images, but clouds prevented any further data acquisition.

Table 2.3. Stars Used for Pointing Offsets

Star	Right Ascension (hh mm ss)	Declination (dd mm ss)
HR 4550	11 52 59	37 43 07
β Leo	11 49 04	14 34 19
SAO 138917	12 41 40	-01 26 58
HD 109085	12 32 06	-16 11 00

We calculated the plate scale for WIRO following Equation 2.1

$$ps = \frac{206265}{f \times D}(arcsec/mm) \tag{2.1}$$

where f is the telescope focal ratio, which for WIRO is 27, and D the primary diameter in mm. For WIRO, D = 2300, so the plate scale is 3.32 arcsec/mm. POETS has 16μm pixels, and so the plate scale becomes 0.053 arcsec/pixel. With a 512 $\times$ 512 CCD, the POETS field of view at WIRO measures approximately 27.1 $\times$ 27.1 arcsec. This field of view is small enough that only one to two stars would span the entire chip. As a result, an unnecessarily large number of pixels would span each star, so we chose to bin 4 $\times$ 4 during the observations.

The following night, we began by following the same stars down to HD 109085, approximately 2 degrees in declination away from the target star. We adjusted our focus on HD 109085 and took a series of biases before moving to the occultation star. We began the data sequence on the occultation star at 06:10:30 UTC, binning 4$\times$4. We had begun a series 5 minutes earlier but did not set the binning properly. The weather was partly cloudy and Pluto's low declination and consequently low altitude made focusing difficult. Clouds also caused significant gaps in usable data. We stopped the sequence approximately 25 minutes after the predicted midtime, at which point the star was completely clouded out. We took a series of biases, flats using the flat screen and dome lights, and more biases. Table 2.4 summarizes our observations on the occultation night, and Figure 2.5 displays an image from the occultation data series.

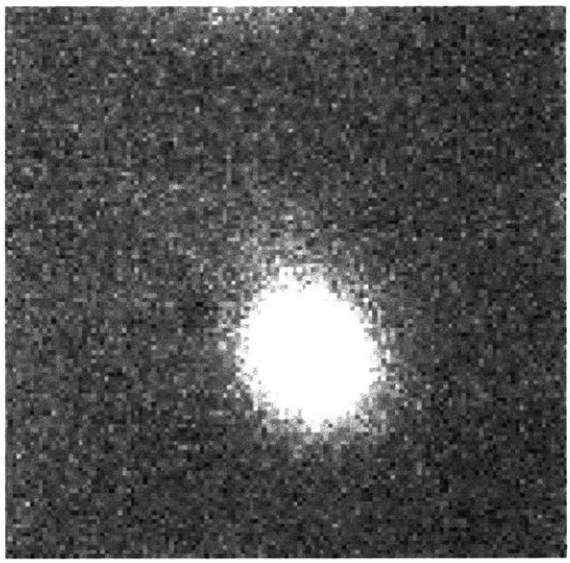

Figure 2.5: ***WIRO Occultation Data Image*** *An image from the occultation data series taken at WIRO. The field of view is approximately 27×27 arcsecs and the binning factor is 4×4.*

Table 2.4. WIRO Observations Summary

Type	Trigger	Δt (s)	Time (UTC)	#	Object/file	Binning	Focus
2011 05 21							
Flat	Internal	0.28557	01:36:00	100	flat / 001	1×1	N/A
Bias	Internal	0.28557	01:41:00	100	bias / 002	1×1	N/A
2011 05 22							
Light	External	0.3	04:10:00	50	HD 109085 / 004	1×1	0.44
Bias	Internal	0.28557	05:11:00	50	bias / 005	1×1	N/A
Light	External	5	06:05:00	54	Pluto / 006	1×1*	0.43
Light	External	5	06:10:30	437	Pluto / 007	4×4*	0.43
Bias	Internal	0.07357	06:49:00	100	bias / 008	4×4	N/A
Flat	Internal	0.07357	06:57:00	250	flat / 009	4×4	N/A
Bias	Internal	0.07357	06:58:00	100	bias / 010	4×4	N/A

*We inadvertently set the binning to 1×1 and so restarted the occultation sequence.

The observations at WIRO resulted in a light curve that was too noisy and had too many gaps to prove useful in fitting Pluto's atmosphere. Of the nine sites described previously, MONET did not find the correct field and so did not obtain occultation star data during the predicted event time. WAO and CCO were completely clouded out and thus did not obtain data either. Additionally, OMM did not start observations until 06:37:00 UT, after the predicted midtime. SVH took data but clouds rendered them unusable. Despite the low quality of the data at some sites, I generated light curves for all six sites that observed occultation star regardless of the start time and gaps, following the procedure outlined in the next chapter.

Chapter 3

Reduction and Analysis

3.1 Light Curve Generation

I performed aperture photometry on the bias, dark and flat corrected images using the **jleGroup** Mathematica image processing packages, utilizing square apertures of various sizes in order to measure the combined Pluto and occultation star signal in one aperture. I generated light curves over several comparison stars and chose for each observation site the aperture and comparison star in which the unocculted (unvarying) signal possessed the highest signal to noise ratio. Table 3.1 displays the signal to noise ratio for each light curve. Note that although OMM possessed a high signal to noise ratio, observations at that site did not begin until 06:37:00 UT, too late after the predicted midtime of 06:22:42 UT to observe the event.

Generating error bars using the internal errors resulted in errors too small given the standard deviation of the occultation star signal outside the event. This could have been caused by underestimation of sources of error such as sky noise or read noise. Therefore I utilized the external errors to generate error bars. For each site, I calculated the standard deviation / mean for the unocculted stellar signal, and then for each point in the light curve, assigned an error bar that was the signal times that ratio. This process resulted in light curves normalized to the flux of the chosen comparison star.

WIRO was the exception to this process in that the field of view was so small that

Table 3.1. Light Curve Signal to Noise

Site[a]	S/N
Williams	**24**
OMM	24
Middlebury	**22**
Yerkes	**16**
SVH	4
WIRO	2

[a]Successful sites bold

only the target star fit in the frame, so no comparison stars were available. Of the six sites that recorded the event, three produced light curves that showed a discernible drop in stellar flux: Middlebury, Williams, and Yerkes, displayed in Figure 3.1. Thus, I chose to fit these three for Pluto's atmosphere. Due to clouds and lack of data at the occultation midtime, the other light curves (WIRO, SVH, and OMM), which can be seen in Figure 3.2, could not be used for atmospheric fitting.

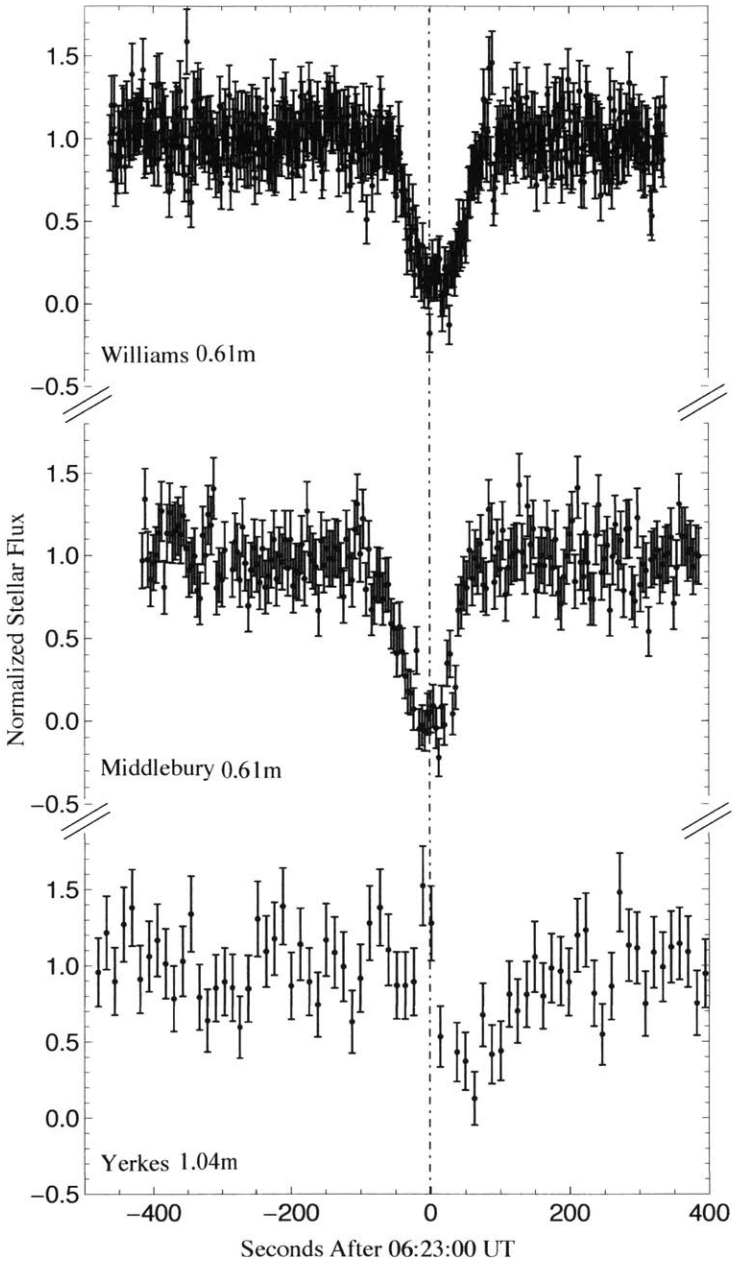

Figure 3.1: ***Fitted Light Curves*** *From top to bottom: Williams, Middlebury, Yerkes. The telescope aperture diameter is listed in the bottom left corner of each panel. The dashed line is for reference and represents the approximate predicted event midtime (∼06:23:00 UT), although the specific midtime varied from site to site.*

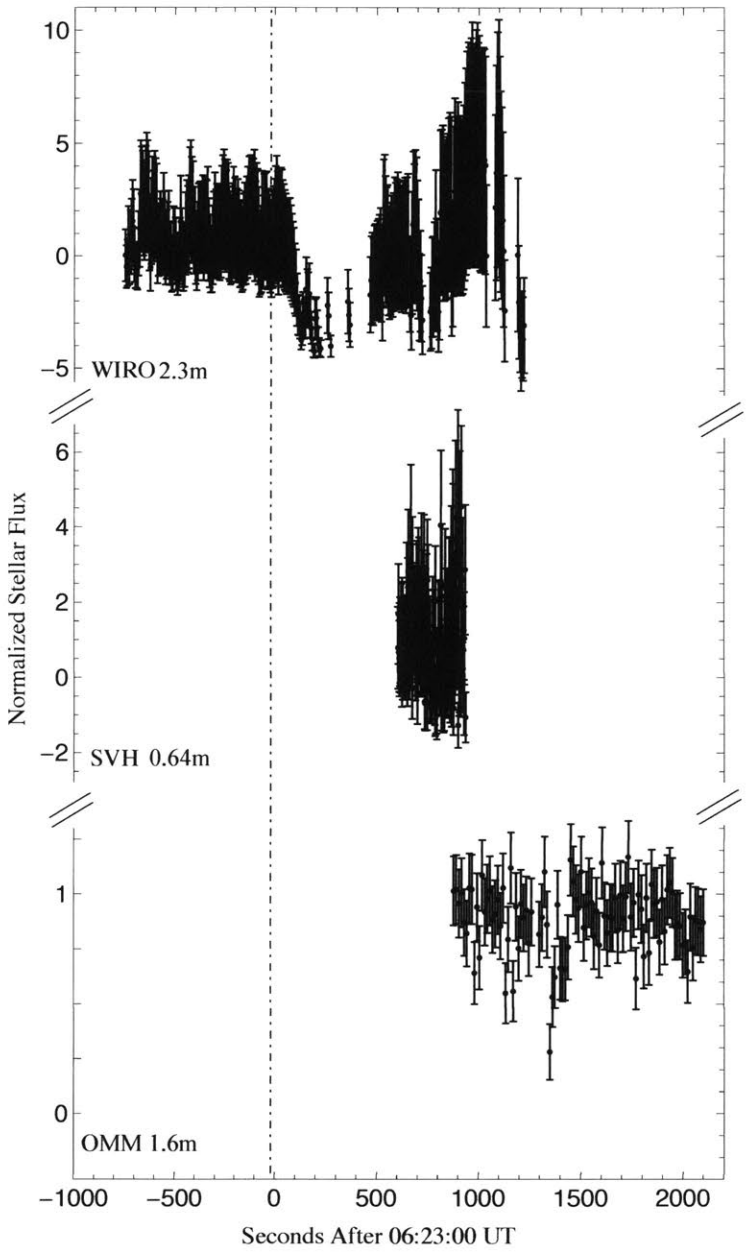

Figure 3.2: ***Unfitted Light Curves*** *From top to bottom: WIRO SVH, OMM. The telescope aperture diameter is listed in the bottom left corner of each panel. The dashed line is for reference and represents the approximate predicted event midtime (∼06:23:00 UT), although the specific midtime varied from site to site.*

3.2 Normalization

Light curves used in atmospheric fitting required normalization in order to account for baseline signal levels due to background light - i.e. light from Pluto, the occulting object. If no baseline signal came from sources other than the occultation star, an occultation light curve normalized to the stellar signal would exhibit a flat baseline at a normalized stellar flux of 1 that would drop down to 0 at the occultation midtime. However, the light curves did not behave in this way - the normalized stellar flux did not drop to zero at the occultation midtime - and thus some of the baseline came from sources other than the target star. Calibration of the light curves to account for this added baseline required independent measurements of the flux from Pluto and the occultation star.

Five calibrated astrometry frames of Pluto separated from the occultation star taken at Magdalena Ridge Observatory (MRO) provided data for absolute light curve normalization. Figure 3.3 shows one of these astrometry frames. Aperture photometry using the **jleGroup** Mathematica packages at a variety of apertures yielded the ratio of Pluto's flux to the flux of the occultation star. I chose the aperture with the highest signal to noise ratio (of 148) and averaged the 5 flux ratios to find a mean Pluto to occultation star flux ratio.

From the Pluto to occultation star ratio, I calculated the background fraction, defined as the percentage of the full occultation baseline signal due to background light. If:

$$r = \frac{pc}{oc} \tag{3.1}$$

where pc = flux from Pluto-Charon and oc = flux from the occultation star, the background fraction (bf) is then:

$$bf = \frac{r}{r+1} \tag{3.2}$$

where r is defined in 3.1.

Before I normalized the light curves using the background fraction, I fit a straight line to each light curve baseline, with the exception of the WIRO light curve since a

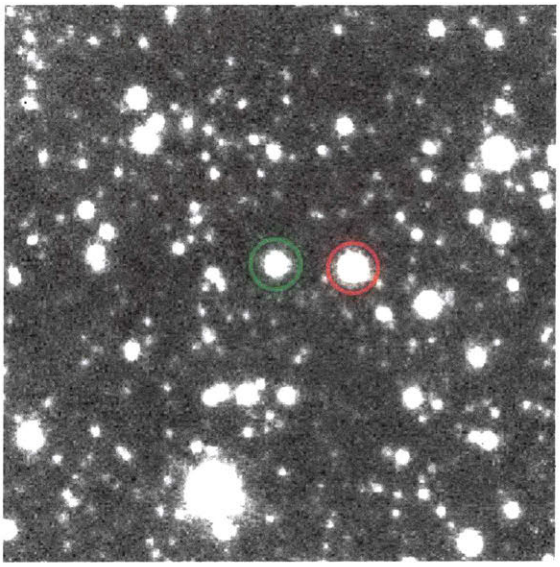

Figure 3.3: ***Normalization Data Frame*** *One of the normalization frames taken from the MRO astrometry data. Pluto is circled in red and the occultation star is circled in green.*

quadratic better fit the baseline. The slope, assumed to be the result of changes in sky brightness during the event, was then subtracted from all data points including the occultation event itself. I then divided the flux value by the zeroth order fit term in order to cause the baseline to correspond as closely as possible to 1. Subtracting the calculated background fraction, and dividing by 1 minus the background fraction yielded light curves in which the baseline should lie at 1, and the lowest occultation point should fall to 0. Equation 3.3 describes this process:

$$nd = \frac{(\frac{(ud-s)}{b} - bf)}{1 - bf} \tag{3.3}$$

Where nd is normalized data, ud is unnormalized data, s is the first order term from the baseline fit, b is the zeroth order term from the baseline fit, and bf is the background fraction. Evaluation of these equations yielded a background fraction of 0.730 ± 0.004.

3.3 Model Fitting

I utilized an empirical model fully described in Elliot and Young [1992] to fit for Pluto's atmosphere. The model assumes the atmosphere is divided into two zones: an upper, clear layer atop a lower layer dominated by either a sharp thermal gradient or extinction. As used in Elliot et al. [2007], the nature of this lower zone does not influence the results of the model fitting, since the model fits the upper atmosphere only.

The model takes into consideration several assumptions relevant to Pluto's atmosphere in particular: (1) the observed light at a given time corresponds to one and only one point on the planetary limb, (2) gravitational acceleration is greater than rotational acceleration in the atmosphere, (3) Pluto's shadow's velocity remains constant throughout the event, (4) Pluto's atmospheric structure maintains spherical symmetry (Elliot and Young [1992]).

I carried out the fitting in Mathematica, using the **jleGroup** Mathematica function **olcTwoLimb4**. Table 3.2 lists the parameters taken by the model light curve.

Table 3.2. Fit Parameters

s_b	Background Level
s'_b	Background Slope
s_f	Full-scale Level
Δt	Integration Time
v	Shadow Velocity
t_{mid}	Midtime
λ_{hi}	Equivalent Isothermal Energy Ratio ($\frac{\mu m_{amu} G M_p}{kTr}$)
b	Temperature Power Index
ρ_{min}	Minimum Observer Radius
r_H	Half-light Radius
$r_{Surface}$	Pluto Surface Radius
r_1	Top of Haze
r_2	$\tau = 1$ Radius
$H_{\tau 1}$	Haze Scale Height

Before fitting, I scaled the normalized stellar flux (which ranged from approximately 0 to 1) by 10000. Thus, of the light curve specific parameters, the background and full-scale levels should have fallen at 0 and 10000 had the light curves been normalized perfectly. However, since the normalization data originated from a site other than Williams and Middlebury, determination of the normalization's reliability required fitting these two parameters for each light curve. The integration time and shadow velocity are constants and are specific to the different observing sites. The equivalent isothermal energy ratio, λ_{hi} is simply the ratio of the gravitational potential energy to k (Boltzmann's constant) multiplied by $T_{isothermal}$ (Pluto's atmospheric temperature were it isothermal), since gravitational acceleration is much greater than rotational atmospheric acceleration. I held λ_{hi} constant throughout the initial fitting, fixing it to 18.3, a value determined in Elliot et al. [2007] from a 2006 Pluto occultation. I later allowed λ_{hi} to go free, but this resulted in unphysically low fit values. The minimum observer radii are specific to each observation site, and, as shown in Figure 3.4 should differ by the difference in sites' distances from the predicted shadow centerline. For all fitting, I held Pluto's surface radius to 500 km, a value small enough that it would be sure not to interfere with determination of the atmospheric radius. I excluded the three haze layer parameters, r_1, r_2, and $H_{\tau 1}$, setting them to Null in all fits since they are specific to the lower atmospheric layer; I have left them out of all subsequent fit tables.

The noise present in the Yerkes light curve prevented a reliable individual fit. Thus to begin, I fit Williams and Middlebury separately, fixing all atmospheric parameters and letting s_b, s_b', s_f, t_{mid}, and ρ_{min} go free in order to quantify the reliability of our normalization and to fit each light curve for the minimum observer radius. Table 3.3 displays the results of this fit. All parameters listed as fixed in Table 3.3 were kept fixed at those values during subsequent fits.

Middlebury was predicted to be located 989 km south of the shadow's centerline, while Williams was 1056 km south. Thus, the resultant ρ_{min}s from their separate fits should differ by 67 km, with Williams the larger of the two. Since they in fact differ by 58 ± 88 km, after I fit the light curves individually, I fit them simultaneously several times, fixing the two ρ_{min}'s based first on the results of the Williams individual fit,

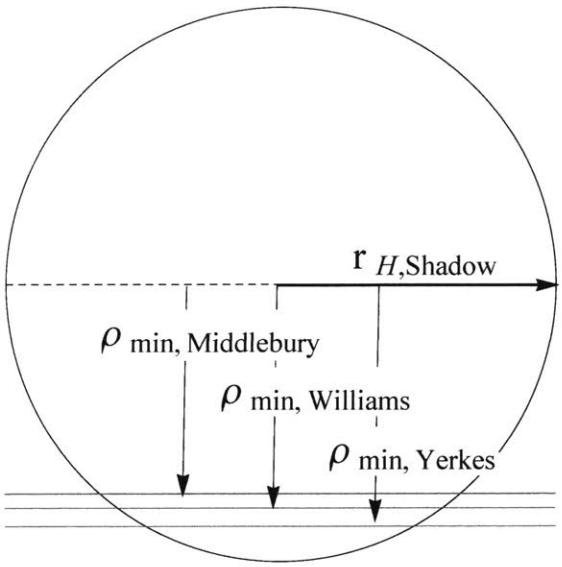

Figure 3.4: ***Minimum Observer Radii*** *Differences in the minimum observer radii pictured as measured chords on Pluto's shadow. From bottom to top the three chords represent Yerkes, Williams, and Middlebury, respectively. The difference between Yerkes' and Williams' ρ_{min}s should be 87 km, and the difference between Williams' and Middlebury's 67 km.*

Table 3.3. Individual Light Curve Fits

Parameter	Williams	Middlebury
Fixed Parameters		
r_H (km)	1291.1	1291.1
λ_{hi}	18.3	18.3
b	-2.2	-2.2
v (km/s)	18.5	18.4
Δt	2	4
$r_{Surface}$ (km)	500	500
Fitted Parameters		
s_b	0.2 ± 0.12	0.2 ± 0.11
s'_b	-0.7 ± 0.34	-0.5 ± 0.48
s_f	9817 ± 89	9746 ± 122
t_{mid} (s)[a]	9.7 ± 1.57	-9.2 ± 2.34
ρ_{min} (km)	902 ± 52	843 ± 70
Reduced Chi Squared		
	0.83	0.88

[a]Measured relative to 06:23:00 UT

and then on the results of the individual Middlebury fit. As discussed in Elliot et al. [2007], the atmospheric model fits the structure of Pluto's upper atmosphere (not lower), and thus model points corresponding to normalized stellar fluxes lower than 0.4 (scaled stellar fluxes lower than 4000) fall higher than the data. Therefore, I fit the atmospheric parameters using only the data points corresponding to normalized stellar fluxes higher than 0.4 (scaled stellar fluxes higher than 4000).

Since, in the individual fits, neither the background nor full-scale levels were within an error bar of 0 and 10000, respectively, I found it necessary to include those light curve parameters in the reference fits. A slope in the light curve full-scale level or an unreliable normalization could have led to these discrepancies. Since the fits returned a non-zero slope for all three light curves and the normalization data are not low quality, I would ascribe the background and full-scale levels to slopes. The first set of reference fits included only the Williams and Middlebury data, which had better signal to noise than the Yerkes data. Table 3.4 summarizes these results. Changing which individual ρ_{min} set the ρ_{min}s in the reference fit only changed r_H by approximately 6 km. The two reference fits are in good agreement. In addition to these two fits, I also fit the light curves with each ρ_{min} value + and − its errors (52 and 70 for Williams and Middlebury, respectively). These fits showed that increasing the ρ_{min}s by an error bar increases r_H by almost two error bars. This behavior of r_H with ρ_{min} provided evidence for the reliability of the fitting. Table A.1 and Table A.2 display these additional fit results.

Following these fits, I fit the data again, this time including the Yerkes data; Table 3.5 summarizes these fit results. Again, the two fits are in good agreement, with r_Hs only differing by 6 km. I chose the adopted fit to be the one with ρ_{min}s fixed by the value from Williams' initial fit, since the errors in Williams' ρ_{min} were smaller than Middlebury's. This adopted fit is shown in bold in Table 3.5. Figure 3.5 shows the data plotted with the adopted model.

Table 3.4. Two Light Curve Fits

Parameter	Fit 1	Fit 2
Williams Lightcurve Parameters		
s_b	0.2 ± 0.09	0.2 ± 0.09
s'_b	-0.7 ± 0.34	-0.7 ± 0.34
s_f	9819 ± 89	9819 ± 89
t_{mid} (s)[a]	9.7 ± 1.60	9.7 ± 1.60
ρ_{min}	902	910
Middlebury Lightcurve Parameters		
s_b	0.2 ± 0.08	0.2 ± 0.08
s'_b	-0.5 ± 0.47	-0.5 ± 0.47
s_f	9751 ± 118	9751 ± 118
t_{mid} (s)[a]	-9.4 ± 2.33	-9.4 ± 2.33
ρ_{min} (km)	835	843
Atmospheric Parameters		
r_H (km)	1295 ± 25	1300 ± 25
Reduced Chi Squared		
	0.85	0.85

[a]Measured relative to 06:23:00 UT

Table 3.5. Three Light Curve Fits

Parameter	**Fit 1**	Fit 2
Williams Lightcurve Parameters		
s_b	**0.2 ± 0.08**	0.2 ± 0.08
s_b'	**−0.7 ± 0.34**	−0.7 ± 0.34
s_f	**9826 ± 90**	9826 ± 90
t_{mid} (s)[a]	**9.7 ± 1.67**	9.6 ± 1.67
ρ_{min} (km)	**902**	911
Middlebury Lightcurve Parameters		
s_b	**0.3 ± 0.08**	0.3 ± 0.08
s_b'	**−0.3 ± 0.46**	−0.3 ± 0.46
s_f	**9783 ± 118**	9784 ± 118
t_{mid} (s)[a]	**−9.6 ± 2.39**	−9.6 ± 2.39
ρ_{min} (km)	**835**	843
Yerkes Lightcurve Parameters		
s_b	**0.2 ± 0.15**	0.2 ± 0.15
s_b'	**0.6 ± 0.95**	0.6 ± 0.95
s_f	**9761 ± 261**	9760 ± 261
t_{mid} (s)[a]	**61.7 ± 5.43**	61.7 ± 5.44
ρ_{min} (km)	**989**	997
Atmospheric Parameters		
r_H (km)	**1309 ± 25**	1314 ± 25
Reduced Chi Squared		
	0.86	0.86

[a]Measured relative to 06:23:00 UT

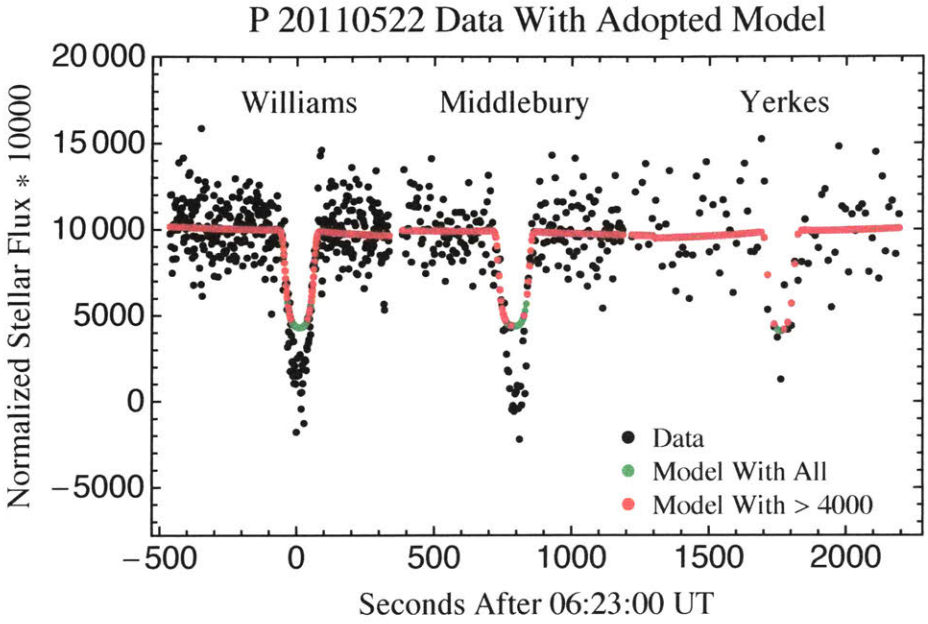

Figure 3.5: ***Data and Adopted Model*** *Adopted model plotted with Williams and Middlebury light curves. Model points used in the fitting (with normalized stellar fluxes greater than 4000) are shown in red. Model behavior for lower fluxes is shown in green. The Middlebury light curve has been shifted by 800 seconds and the Yerkes light curve by 1700 seconds.*

Using λ_{hi}, the isothermal energy ratio, and b, the temperature power index, I calculated the λ_h, ratio of gravitational potential energy to kT_h, where T_h represents Pluto's atmospheric temperature at the half-light radius, r_h, using Equation 3.4, from Elliot et al. [2003a].

$$\lambda_h = \lambda_{hi} - \frac{5b}{2} \tag{3.4}$$

Calculation of λ_h allowed for calculation of H, Pluto's pressure scale height, as well as T_h, the temperature at the half light radius, r_h, using Equations 3.5 and 3.6, respectively, from Elliot et al. [2003a].

$$H = \frac{r_h}{\lambda_h} \tag{3.5}$$

Table 3.6. Adopted Fit: Derived Parameters

Parameter	Adopted Value
r_H (km)	1309 ± 25
λ_h	23.8
H (km)	55 ± 2
T_h (K)	94 ± 4

$$T_h = \frac{\mu m_{amu} G M_p}{r_h k \lambda_h} \tag{3.6}$$

Where μ represents the atmosphere's mean molecular weight, $m_{amu} = 1.66030 \times 10^{-27}$ the atomic mass unit in kg, $G = 6.67320 \times 10^{-11}$, the gravitational constant, $M_p = 1.305 \times 10^{22}$ kg Pluto's mass, and k= 1.38062×10^{-23} Boltzmann's constant. In using equation 3.6 I assumed Pluto's atmosphere is composed entirely of N_2, with mean molecular weight $\mu = 28.01$ amu. The value for Pluto's mass was taken from Elliot et al. [2003a]. Table 3.6 displays the derived parameters from the adopted fit.

Chapter 4

Discussion

4.1 Goodness of Fit

The reduced chi squared values displayed in all of the fit tables in the previous chapter are approximately 0.85 - 0.86. Having a low (< 1) reduced chi squared like this indicates that the model is "over-fitting" the data, that the errors have been overestimated. This is likely a result of my decision to utilize the external rather than internal errors. However, I did carry out the fitting using the unreasonably small internal errors initially, and this resulted in reduced chi squared values ranging between 2.5 and 5.5. Thus, utilizing the light curves with the external errors still resulted in more realistic parameter error bars and a better fit.

4.2 Site Specific Parameters

The first site specific parameters to examine are the ρ_{min} values from the Williams and Middlebury individual light curve fits, which determined the ρ_{min}s used to carry out the simultaneous fits. The predicted distance between the two sites with respect to Pluto's center was 67 km, with Williams farther from the centerline. Thus, $\rho_{min,Williams}$ should be greater than $\rho_{min,Middlebury}$ by 67 km. The difference between the two is in fact 58 ± 88 km. The large errors stem from the fact that the individual ρ_{min} fits possessed large error bars due to the noise present in the light curves. Since

the $\rho_{min,Williams}$ error was much less than the $\rho_{min,Middlebury}$ error, I fixed the ρ_{min} values based on Williams' individual fit. However, I did carry out the fitting based on Middlebury's individual fit; see Table 3.5 (Fit 2) as well as Table A.2 for these results.

Examination of the s_b, s'_b, and s_f values in the three light curve fits reveals a full scale level not within an error bar of 10000 and a background level not within an error bar of zero for all three light curves. This could either be the result of inadequate normalization, perhaps due to poor measurement of Pluto-Charon signal separated from the occultation star signal. It could also be due to a slope in the full scale level. I think this is the more likely case; I am confident in the quality of the normalization data. While I did fit a straight line to the non-occulted signal while producing the light curves, this could have been insufficient in subtracting background variation. The fitted slope then represents whatever slope was left over after the normalization process.

Table 4.1 lists predicted and fitted midtimes for the three sites. The adopted fit resulted in a difference of 19.2 $\pm$ 2.91 seconds between Williams and Middlebury (with Williams later), and a difference of 52.0 $\pm$ 5.93 seconds between Yerkes and Williams (with Yerkes later). The predicted differences between the midtimes were Middlebury 2 seconds later and Yerkes 57 seconds later than Williams. The adopted difference between Williams and Yerkes better agrees with the predictions than the difference between Williams and Middlebury. Midtime fit issues such as these could have resulted from low time resolution in the light curves. Williams possessed highest cadence of the three, at 0.5 Hz, followed by Middlebury's 0.25 Hz, and then Yerkes at 0.08 Hz. Noise presents itself as another obvious source of timing issues; a noisy data point falling well above or well below 0 around the event midtime could cause a less reliable fit.

4.3 Atmospheric Parameters

Table 4.2 displays the results of this paper alongside four previous Pluto occultation fits. As stated in the previous chapter, λ_{hi} and consequently, λ_h were fixed based

Table 4.1. Midtimes

Site	Predicted Midtime hh:mm:ss UT	Adopted Midtime hh:mm:ss UT
Williams	06:23:44	06:23:10 ± 00:00:02
Middlebury	06:23:46	06:22:50 ± 00:00:02
Yerkes	06:24:41	06:24:02 ± 00:00:05

on the result from Elliot et al. [2007]. I did this in order to stabilize the fit; fitting with λ_{hi} free resulted in unphysical values. The half-light radius in the atmosphere is within an error bar of the fit parameters from the March 18, 2007 event. The changes in half light radius since 1988 imply three epochs in Pluto's atmosphere, with a significant increase between the 1988 and 2002 events, an increase between the 2006 and 2007 events, and little change since 2007.

Over the five events listed since 1988 the pressure scale height has not changed significantly, despite the changes in half-light radius. The changes in temperature account for this consistent scale height and fluctuating half-light radius; as half-light radius has increased during the last 23 years, temperature has decreased, allowing the scale height to remain relatively constant.

4.4 Implications for Pluto's Atmosphere

The upper panel of Figure 4.1 displays Figure 7 from Elliot et al. [2007], showing the first three occultation shadow radii plotted against one of the frost migration models published in Hansen and Paige [1996]. Elliot et al. [2007] hypothesized that the dramatic increase in shadow radius supports the existence of frost migration on Pluto, where Pluto's surface has a low thermal inertia. The lower panel of FIgure 4.1 displays the shadow radii from all five fitted occultations to date, where the shadow radii are found by subtracting a single scale height from the atmospheric half light radii. While the first three events from Elliot et al. [2007] match the model well,

Table 4.2. Pluto's Upper Atmosphere: 1988 - 2011

Parameter	1988 June 9[a]	2002 August 21[a]	2006 June 12[b]	2007 March 18[c]	2011 May 22
Half-light radius (km)[d,e]	1233 ± 4	1279 ± 5	1276 ± 4	1291 ± 5	1309 ± 25
Pressure scale height (km)[e,f]	56 ± 5	61 ± 4	54 ± 3	54.2 ± 0.2	55 ± 2
Temperature (K)[e,f]	114 ± 10	108 ± 9	97 ± 5	95 ± 1	94 ± 4

[a]After Person et al. [2008]

[b]From Elliot et al. [2007]

[c]From Person et al. [2008]

[d]In Pluto's atmosphere (not the shadow)

[e]At the half-light radius

[f]For an N_2 atmosphere

the additional shadow radii do not. Hansen and Paige [1996] published many more models in which they varied parameters such as the thermal inertia of Pluto's surface, the substrate and frost albedo, the frost emissivity, and the supply of N_2. While the change from 1988 to 2002 suggests a low thermal inertia (1×10^3 cal/K cm^2 sec$^{1/2}$) model fits the data better than a high thermal inertia model ($7 - 50 \times 10^3$ cal/K cm^2 sec$^{1/2}$), the best fit values for the remaining parameters remain unknown. Changing those parameters dramatically changes the model behavior over the 1970 - 2020 time period.

Between 1988 and 2011, Pluto's shadow radius has been increasing, at times more dramatically than others. Only after the 2006 event have enough data points accumulated to show that the frost migration model used as an example in Elliot et al. [2007] does not fit the data. This is only one of many models, but in general it is true that better constraints on model parameters other than the thermal inertia values until require more observations.

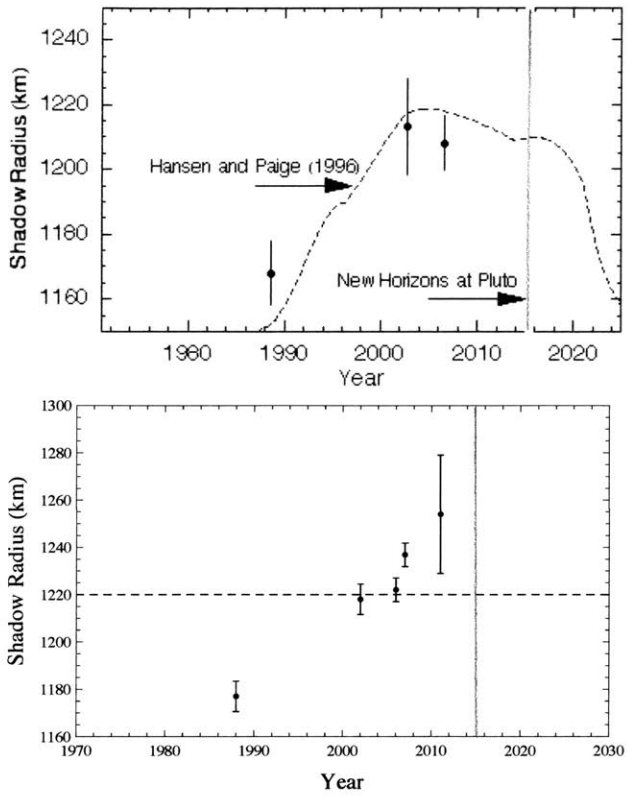

Figure 4.1: ***Shadow Radius Over Time Top Panel:*** *Figure 7 from Elliot et al. [2007]. The 1988, 2002, 2006 half-light shadow radii plotted against one frost migration model from Hansen and Paige [1996].* ***Bottom Panel:*** *Pluto's shadow radius (the half-light radius minus a single pressure scale height) from the five fitted occultations since 1988. The horizontal line is for reference, marking roughly the highest value of shadow radius from the frost migration model plotted above. Vertical lines in both plots indicate the arrival of the* New Horizons *spacecraft. Note that the second and third points are inconsistent between the two plots; this likely resulted from the fact that in this paper, I calculated the shadow radius for each event by subtracting that event's scale height from the half-light radius in the atmosphere. In the 2007 figure, the shadow radii were calculated by subtracting a constant scale height from the half-light radius in the atmosphere.*

Chapter 5

Conclusion

We attempted observations of the 22 May 2011 stellar occultation by Pluto from nine sites across the United States. Due to weather conditions, only three successfully recorded the event. I reduced the data, producing light curves that I then simultaneously fit for Pluto's atmospheric parameters.

The atmospheric fit results indicated that Pluto's atmosphere has remained relatively stable since the dramatic increase recorded between 1988 and 2002, although the half-light radius has slowly increased since then. While none of these increases have occurred as dramatically as the first, the 12 June 2006 and 18 March 2007 events revealed an increase slightly outside the half-light radius error bars (from 1276 $\pm$ 4 km to 1291 $\pm$ 5 km), suggesting three epochs in Pluto's atmosphere since 1988. The result from this event (1309 $\pm$ 25 km) is consistent with the 18 March 2007 half-light radius.

While the half-light radius increased gradually between 2002 and 2011, the pressure scale height remained constant, implying that a gradual decrease in temperature balanced the increasing half-light radius.

Comparison of the current shadow radii with a frost migration model from Hansen and Paige [1996] shows that while the increase between 1988 and 2002 requires Pluto's surface to possess a low thermal inertia, constraining the other frost migration model parameters requires additional data. Future observations of stellar occultations will provide a better means of understanding the mechanism by which Pluto's atmosphere

evolves. This event and those previous indicate that the *New Horizons* scheduled fly by in 2015 will find a dynamic atmosphere around Pluto.

Bibliography

Artigau, E. et al. (2004), CPAPIR: A wide-field infrared camera for the Observatoire du Mont Megantic. *Proc. SPIE 5492,* 1479.

Brosch, N. (1995), The 1985 stellar occultation by Pluto. *Mon. Not. R. Astron. Soc. 276,* 571-578.

Elliot, J. L., Young, L. A., (1992), Analysis of stellar occultation data for planetary atmospheres. I. Model fitting, with application to Pluto. *Astron. J. 103,* 991-1015.

Elliot, J. L. et al. (1989), Pluto's atmosphere. *Icarus 77,* 148-170.

Elliot, J. L., Person, M. J., Qu, S., (2003), Analysis of stellar cccultation data. II. Inversion, with application to Pluto and Triton. *Astron. J. 126,* 1041-1079.

Elliot, J. L. et al. (2003), The recent expansion of Pluto's atmosphere. *Nature 424,* 165-168.

Elliot, J. L., et al. (2007), Changes in Pluto's atmosphere: 1988 - 2006. *Astron. J. 134,* 1-13.

Eshleman, V. R., (1989), Pluto's atmosphere: models based on refraction, inversion, and vapor pressure equilibrium. *Icarus 80,* 439-443.

Gulbis, A. A. S. et al. (2008), in The Universe at Sub-Second Timescale, High Time Resolution Astrophysics, Recent Stellar Occultation Observations Using High-Speed, Portable Camera Systems, ed. D. Phelan, O.Ryan, & A. Shearer (Edinburgh: American Institute of Physics), 91.

Hansen, C. J., Paige, D. A. (1996), Seasonal Nitrogen Cycles on Pluto. *Icarus 120,* 247-265.

Hubbard, W. B., Yelle, R. V., Lunine, J. I., (1990), Nonisothermal Pluto atmosphere models. *Icarus 84,* 1-11.

Lockhart, M. et al. (2010), PICO: Portable instrument for capturing occultations. *PASP 122,* 1207-1213.

Millis, R. L. et al. (1993), Pluto's radius and atmosphere: results from the entire June 9 1988 data set. *Icarus 105,* 282-297.

Owen, T. C. et al. (1993), Surface ices and the atmospheric composition of Pluto. *Science 261,* 745-749.

Pasachoff, J. M. (2005), The structure of Pluto's atmosphere from the 2002 August 21 stellar occultation. *Astron. J. 129,* 1718-1723.

Person, M. J. et al. (2008), Waves in Pluto's upper atmosphere. *Astron. J. 136,* 1510-1518.

Person, M. J. et al. in prep.

Sicardy, B. et al. (2003), Large changes in Pluto's atmosphere as revealed by recent stellar occultations. *Nature 424,* 168-170.

Souza, S. P. et al. (2006), POETS: Portable occultation, eclipse, and transit system. *PASP 118,* 1550-1557.

Stansberry, J. A. (1994), Mirages and the nature of Pluto's atmosphere. *Icarus 111,* 503-513.

Yelle, R. V., Lunine, J. I. (1989), Evidence for a molecule heavier than methane in the atmosphere of Pluto. *Nature 339,* 228-230.

Appendix A

Additional Light Curve Fits

Table A.1 and table A.2 list additional preliminary fits used to arrive at the adopted fit. Table A.1 lists the results of fitting the data twice, using $\rho_{min,Williams} \pm$ its error of 52.17 km, and Table A.2 lists the results of fitting the data twice, using $\rho_{min,Middlebury} \pm$ its error of 70.34 km. In both sets of fitting, increasing the ρ_{min} by two error bars increased r_H by more than twice it's error bar.

Table A.1. Three Light Curve Reference Fits 1

Parameter	Fit 1[a]	Fit 2[b]
Williams Lightcurve Parameters		
s_b	0.2 ± 0.08	0.2 ± 0.09
s'_b	-0.7 ± 0.34	-0.7 ± 0.34
s_f	9826 ± 90	9826 ± 90
t_{mid}	9.7 ± 1.65	9.6 ± 1.69
ρ_{min}	849	954
Middlebury Lightcurve Parameters		
s_b	0.3 ± 0.08	0.2 ± 0.08
s'_b	-0.3 ± 0.46	-0.3 ± 0.46
s_f	9782 ± 118	9784 ± 118
t_{mid}	-9.5 ± 2.35	-9.6 ± 2.43
ρ_{min}	782	887
Yerkes Lightcurve Parameters		
s_b	0.2 ± 0.15	0.2 ± 0.16
s'_b	0.6 ± 0.95	0.6 ± 0.95
s_f	9764 ± 261	9758 ± 261
t_{mid}	61.5 ± 5.32	61.9 ± 5.53
ρ_{min}	936	1041
Atmospheric Parameters		
r_H	1277 ± 25	1341 ± 25
Reduced Chi Squared		
	0.86	0.86

[a] $\rho_{min,Williams}$ - its error of 52 used to set all three ρ_{min} values

[b] $\rho_{min,Williams}$ + its error of 52 used to set all three ρ_{min} values

Table A.2. Three Light Curve Reference Fits 2

Parameter	Fit 1[a]	Fit 2 [b]
Williams Lightcurve Parameters		
s_b	0.2 ± 0.08	0.2 ± 0.09
s'_b	-0.7 ± 0.34	-0.7 ± 0.34
s_f	9826 ± 90	9826 ± 90
t_{mid}	9.7 ± 1.65	9.6 ± 1.69
ρ_{min}	840	981
Middlebury Lightcurve Parameters		
s_b	0.3 ± 0.08	0.2 ± 0.08
s'_b	-0.3 ± 0.46	-0.3 ± 0.46
s_f	9782 ± 118	9785 ± 118
t_{mid}	-9.5 ± 2.34	-9.7 ± 2.45
ρ_{min}	773	914
Yerkes Lightcurve Parameters		
s_b	0.2 ± 0.15	0.1 ± 0.16
s'_b	0.6 ± 0.95	0.6 ± 0.95
s_f	9765 ± 261	9756 ± 261
t_{mid}	61.5 ± 5.30	62.0 ± 5.59
ρ_{min}	927	1068
Atmospheric Parameters		
r_H	1271 ± 25	1358 ± 25
Reduced Chi Squared		
	0.86	0.86

[a] $\rho_{min,Middlebury}$ - its error of 70 used to set all three ρ_{min} values

[b] $\rho_{min,Middlebury}$ + its error of 70 used to set all three ρ_{min} values